Electronic Supplementary Material (ESI) for Polymer Chemistry.

Supporting Information

Controlling Biofilm Formation with Nitroxide Functional Surfaces

Hendrik Woehlk,[abc] Michael J. Trimble,[c] Sarah C. Mansour,[c] Daniel Pletzer,[c] Vanessa Trouillet,[de] Alexander Welle,[ef] Leonie Barner,[ag] Robert E. W. Hancock,[c] Christopher Barner-Kowollik,*[ab] and Kathryn E. Fairfull-Smith*[a]*

[a] School of Chemistry, Physics and Mechanical Engineering, Faculty of Science and Engineering, Queensland University of Technology (QUT), 2 George St, Brisbane, QLD 4000, Australia

[b] Macromolecular Architectures, Institut für Technische Chemie und Polymerchemie, Karlsruhe Institute of Technology (KIT), Engesserstr. 18, 76131 Karlsruhe, Germany

[c] Department of Microbiology and Immunology, Center for Microbial Diseases and Immunity Research, University of British Columbia, Vancouver, BC V6T 1Z4, Canada

[d] Institute for Applied Materials (IAM-ESS), Karlsruhe Institute of Technology (KIT), Hermann-von-Helmholtz-Platz 1, 76344 Eggenstein-Leopoldshafen

[e] Karlsruhe Nano Micro Facility (KNMF), Karlsruhe Institute of Technology (KIT), Hermann-von-Helmholtz-Platz 1, 76344 Eggenstein-Leopoldshafen

[f] Institute of Functional Interfaces (IFG), Karlsruhe Institute of Technology (KIT), Hermann-von-Helmholtz-Platz 1, 76344 Eggenstein-Leopoldshafen

[g] Institute for Future Environments, Queensland University of Technology (QUT), 2 George Street, Brisbane QLD 4000, Australia

*to whom correspondence should be addressed

E-mail: *bob@hancocklab.com; christopher.barnerkowollik@qut.edu.au; k.fairfull-smith@qut.edu.au*

Materials

Ciprofloxacin hydrochloride monohydrate (Sigma-Aldrich, LOT #: LRAA8718, 93.4%), cyclohexylamine (Cy; 99%), dry dichloromethane (dry DCM; 99.8% extra dry), 4-(dimethylamino)pyridine (DMAP; 99%), 1-ethyl-3-(3-dimethylaminopropyl) carbodiimide hydrochloride (EDC·HCl; 98%), tris(hydroxymethyl)methylamine (Tris; 99%) were used as received from Sigma-Aldrich or Acros Organics. Titanium plates (Trinon Titanium, Karlsruhe, Germany) and hydroxyapatite (HA) discs (Clarkson Chromatography Products Inc., South Williamsport, USA) were used as received from their supplier.

Instrumentation and Characterization Methods

***Photoreactor*:** UV-triggered experiments were performed using a Luzchem LZV-4V photoreactor (Luzchem Research Inc., Ottawa, Canada) equipped with 10 UV-B lamps (LZC-UVB, emission centred at approx. 300 nm, with a peak of 313 nm), irradiating from the top and the sides under continuous rotation or stirring of the samples. A custom-made sample holder and a dotted shadow mask (Ø 1 mm pinholes) were employed for photolithographic surface patterning.[1]

***Nuclear magnetic resonance (NMR) spectroscopy*:** ^{1}H NMR (600 MHz) and ^{13}C NMR (151 MHz) spectroscopy was performed on a Bruker Avance III HD spectrometer at 298 K. Chemical shifts are expressed in parts per million (ppm) and coupling constants (*J* values) are reported in hertz (Hz). The *δ* scale is referenced to characteristic (residual) signals of the employed deuterated solvent (*i.e.*, methanol-d_4). Appearances of NMR signals are described as singlet (s), doublet (d), doublet of doublets (dd) and multiplet (m).

***High-resolution electrospray ionization mass spectrometry (HR-ESI MS)*:** Mass spectrometric characterization was performed on a LTQ Orbitrap XL Q Exactive mass spectrometer (Thermo Fisher Scientific, San Jose, CA, USA) equipped with an HESI II probe. The instrument was calibrated in the *m/z* range of 74–1822 using standard calibration solutions (Thermo Scientific) and between *m/z* 1000–6000 with ammonium hexafluorophosphate. The capillary temperature was set to 320 °C, and the S-lens RF level was set to 68.0. A spray voltage of 3.6 kV was employed for (+)ESI. All samples were dissolved in THF/MeOH 3:2 (*v*/*v*) and filtered prior to injection.

***Electron paramagnetic resonance (EPR) spectroscopy*:** EPR spectra were recorded on a Magnettech MiniScope MS400 spectrometer at ambient temperature. Aliquots (50 µL) of the aqueous coating solution were taken for EPR spectroscopic analysis during polymerization of **4**.

***UV–visible (UV–vis) spectroscopy*:** UV–vis spectra were recorded on a Shimadzu UV-2700 UV–vis spectrophotometer in the range of 240–600 nm at ambient temperature. A quartz Suprasil cuvette with a 10 mm light path was employed. UV–vis spectroscopic aliquots (50 µL) were taken during oxidative polymerization of **4** and diluted to 0.1 mM using Tris–HCl buffer prior to spectrophotometric characterization. UV–vis spectra were baseline-corrected with respect to pure Tris–HCl buffer.

***Spectroscopic ellipsometry*:** The determination of the polymer film thicknesses deposited on silicon substrates was performed on a J. A. Woollam M-2000UI Ellipsometer in the wavelength range of 245–1690 nm and at angles of incidences of 65, 70, and 75°. The polymer film thickness was measured at several spots on the surface and averaged. The data were fitted and evaluated using the CompleteEASE software. A Cauchy model was applied for the polymer surface deposition (A = 1.45, B = 0.01, surface roughness excluded) on Si/SiO_x substrates. The SiO_x interlayer was determined prior to surface coatings.

***X-ray photoelectron spectroscopy (XPS)*:** XPS measurements were performed using a K-Alpha+ XPS spectrometer (Thermo Fisher Scientific, East Grinstead, United Kingdom) equipped with a microfocused, monochromated Al K_α X-rays source (400 µm spot size). The kinetic energy of the electrons was measured by a 180° hemispherical energy analyzer operated in the constant analyzer energy mode (CAE) at 50 eV pass energy for elemental spectra. The K-alpha charge compensation system was employed during analysis using electrons of 8 eV energy and low-energy argon ions to prevent any localized charge build-up. The recorded XPS spectra were evaluated using the Thermo Avantage software.[2] The high-resolution spectra were fitted with one or more Voigt profiles (BE uncertainty: ±0.2 eV). The Scofield sensitivity factors were applied for quantification.[3] All spectra were referenced to the C 1s (C–C, C–H) peak at BE 285.0 eV and controlled by means of well-known photoelectron peaks of metallic elements. The K-alpha+ snapmap option permits imaging of an area of 3 × 3 cm^2 using an X-ray spot of 200 µm. 7 iterations were run for better contrast and the data were collapsed in order to get a better signal-to-noise ratio. Afterwards, a principal component analysis of the data was applied for the generation of the XPS images.

***Time-of-flight secondary ion mass spectrometry (ToF-SIMS)*:** ToF-SIMS was performed on a TOF.SIMS 5 instrument (ION-TOF GmbH, Münster, Germany) equipped with a Bi cluster primary ion source and a reflectron type time-of-flight analyzer. The Bi source was operated in the high current

bunched mode providing short Bi_3^+ primary ion pulses at 25 keV energy and a later resolution of approx. 4 µm. The short pulse length of typically 1.3 ns allowed for high mass resolution. The primary ion beam was rastered in individual patches of 500 × 500 μm^2 and the stage scan mode was employed for larger areas with 10 µm pixel distance. Primary ion doses were kept below 10^{11} ions·cm^{-2} (static SIMS limit). Dynamic SIMS experiments were performed using an argon cluster erosion beam. For these experiments, the sample was eroded by an Ar_{1500}^+ beam at 5 keV rastered over 800 × 800 μm^2. A concentric field of view of 500 × 500 μm^2 (the maximum scanning range of the primary ion gun) was imaged continuously. All ToF-SIMS spectra were calibrated on omnipresent (hydro)carbon peaks. For additional information about the dynamic ToF-SIMS experiments refer to Fig. S9–S10.

***Confocal laser scanning microscopy (CLSM)*:** Microscopy was performed using a Zeiss LSM 800 microscope (Carl Zeiss AG, Oberkochen, Germany). Confocal images were evaluated using the Zeiss ZEN software. Substrates were individually background subtracted with respect to the employed underlying type of material.

Experimental Data

Compounds **1**,[4] **2** and **4**[5] were synthesized according to literature-known procedures.

***Synthesis of precursor 3*:** 4-*bis*(*tert*-Butyldimethylsilyloxy)-*N*-*tert*-butyloxycarbonyl-L-phenylalanine (**1**) (5.26 g, 10.0 mmol, 1 eq.), cyclohexylamine (1.72 mL, 15.0 mmol, 1.5 eq.) and 4-dimethylaminopyridine (2.44 g, 20.0 mmol, 2.0 eq.) were dissolved in dry dichloromethane (50 mL). 1-Ethyl-3-(3-dimethylaminopropyl)carbodiimide hydrochloride (3.83 g, 20.0 mmol, 2.0 eq.) was added, and the reaction solution was stirred for 24 h at room temperature followed by extraction with saturated sodium hydrogen carbonate solution (50 mL), deionized water (20 mL) and saturated sodium chloride solution (20 mL). The organic phase was dried over sodium sulfate and the filtrate was evaporated under reduced pressure. The crude product was purified by silica column chromatography employing ethyl acetate and cyclohexane (3:1) as solvent mixture (R_f = 0.56). Compound **3** was isolated a white solid (5.0 g, 8.2 mmol, 82%). M.p. 114 °C; ^{1}H NMR (600 MHz, methanol-d_4) δ (ppm) = 6.76 (d, J = 8.1 Hz, 1H, $C_{Ar}H$), 6.73 (d, J = 2.1 Hz, 1H, $C_{Ar}H$), 6.69 (dd, J = 8.1, 2.1 Hz, 1H, $C_{Ar}H$), 4.15 (m, 1H, C_{Ar}–CH_2–CH), 3.58 (m, 1H, NH–CH(CH_2)$_5$), 2.79 (m, 2H, C_{Ar}–CH_2), 1.86–1.03 (m, 10H, (CH_2)$_5$), 1.40 (s, 9H, O–C(CH_3)$_3$), 1.00 (s, 9H, Si–C(CH_3)$_3$), 0.99 (s, 9H, Si–C(CH_3)$_3$), 0.20 (s, 6H, Si(CH_3)$_2$), 0.19 (s, 6H, Si(CH_3)$_2$); ^{13}C NMR (151 MHz, methanol-d_4) δ (ppm) = 173.0 (C), 157.4 (C), 147.7 (C), 146.9 (C), 131.8 (C), 123.7 (CH), 123.6 (CH), 122.1 (CH), 80.6 (C), 57.5 (CH), 49.7 (CH), 39.1 (CH_2), 33.7 (CH_2), 33.6 (CH_2), 28.7 (CH_3), 26.6 (CH_2), 26.54 (CH_3), 26.53 (CH_3), 26.1 (CH_2), 19.34 (C), 19.31 (C), −3.7 (CH_3), −3.8 (CH_3); HRMS (*m/z*) calculated for $C_{32}H_{58}N_2NaO_5Si_2$ $[M+Na]^+$ 629.3776, found 629.3777.

***Synthesis of coating agent 5*:** All solvents were purged with nitrogen for 15 min prior to usage. Compound **3** (1.82 g, 3.0 mmol, 1.0 eq.) was dissolved in methanol (18 mL) and the solution was cooled to 0 °C. 6 M aqueous HCl (6 mL, 12 eq.) was added dropwise, and the solution was stirred for 6 h and allowed to reach room temperature. The solvent and volatiles were carefully removed under reduced pressure. The crude product was redissolved in water (10 mL, acidified with a few drops of 1 M HCl), filtered and lyophilized. The pure product was isolated after redissolving in water (10 mL) and subsequent lyophilization in quantitative yields as a white powder. M.p. 84 °C; ^{1}H NMR (600 MHz, methanol-d_4) δ (ppm) = 6.74 (d, J = 8.0 Hz, 1H, $C_{Ar}H$), 6.70 (d, J = 2.1 Hz, 1H, $C_{Ar}H$), 6.58 (dd, J = 8.0, 2.1 Hz, 1H, $C_{Ar}H$), 3.91 (m, 1H, C_{Ar}–CH_2–CH), 3.60 (m, 1H, NH–CH(CH_2)$_5$), 2.94 (m, 2H, C_{Ar}–CH_2), 1.89–1.00 (m, 10H, (CH_2)$_5$); ^{13}C NMR (151 MHz, methanol-d_4) δ (ppm) = 168.6 (C), 146.7 (C), 146.1 (C), 126.8 (C), 121.9 (CH), 117.6 (CH), 116.6 (CH), 56.0 (CH), 50.0 (CH), 38.3 (CH_2), 33.5 (CH_2), 33.4 (CH_2), 26.5 (CH_2),

25.9 (CH_2); HRMS (*m/z*) calculated for $C_{15}H_{23}N_2O_3$ $[M-Cl]^+$ 279.1703, found 279.1702. The corresponding ^1H NMR and ^{13}C NMR spectra of compounds **3** and **5** are depicted in Fig. S1 and S2.

***Surface coatings with 4 and 5*:** All coatings employed for the biological studies were conducted under sterile conditions. Compound **4** (51 mg) was dissolved in 100 mM Tris–HCl buffer (3 mL, pH 9.25). Uncoated substrates (hydroxyapatite or titanium) were immersed for 24 h at room temperature under gentle shaking of the coating solution. After coating, the substrates were thoroughly rinsed with water and dried under atmospheric conditions. The reference coating system was prepared likewise employing compound **5** (38 mg) as a coating agent.

***Photopolymerization of 4 with in situ polymer surface deposition*:** Monomer **4** (11 mg, 25 µmol) was dissolved in 10 mM Tris–HCl buffer (5 mL, pH 8.5). The resulting 5 mM coating solution was vigorously stirred in a closed glass vial and exposed to UV-B irradiation for 0–12 h. Aliquots (50 µL) were taken for EPR spectroscopic analysis. UV/vis spectroscopic aliquots (50 µL) were diluted to 0.1 mM prior to spectrophotometric characterization. At the same time, silicon substrates were placed in a petri dish and covered by a separate coating solution. The immersed substrates were exposed to UV irradiation for 0–12 h under continuous rotation of the petri dish in the photoreactor. Coated silicon substrates were analyzed by spectroscopic ellipsometry. The control experiments performed in the dark were conducted likewise. The presented data were obtained from a representative study and may vary in time and intensity due to the initial concentration of dissolved oxygen.

***Photolithographic surface patterning with 4*:** Compound **4** (11 mg, 25 µmol) was dissolved in 10 mM Tris–HCl buffer (5 mL, pH 8.5). Titanium substrates (1 × 1 cm^2) were covered by dotted shadow masks (Ø 1 mm pinholes) and placed in a custom-made sample holder. The partially covered substrates were vertically immersed into the coating solution and exposed to UV irradiation for 12 h. After coating, the patterned surfaces were carefully washed with water and dried under atmospheric conditions.

***Generation and transformation of a plasmid constitutively expressing egfp into Pseudomonas aeruginosa PA14*:** In order to visually track *P. aeruginosa* during biofilm experiments, a plasmid encoding the enhanced green fluorescence protein-encoding gene (*egfp*), under constitutive expression from the *lac* promoter, was constructed (pUCP23.egfp). Therefore, plasmid pBBR1.egfp.TIR[6] was digested with restriction enzyme *Nsi*I and subsequently treated with nuclease S1. Next, the *egfp* gene was excised with *BamH*I. We used as a recipient vector pMCh-23[7] carrying a red fluorescence *mCherry* gene. We removed this gene via *EcoR*I, which was subsequently treated

with nuclease S1, and then further digested using *BamH*I. The resulting backbone vector, pUCP23 was used for ligation of *egfp*. All enzymes were purchased from Thermo Fisher Scientific and the reactions were carried out following the manufacturer's instructions. Successful transformants were verified for *egfp* expression using the Synergy H1 plate reader (BioTek) with an excitation wavelength of 478 nm and emission at 510 nm. The *egfp* expressing plasmid, pUCP23.egfp, was transformed into electrocompetent *Pseudomonas aeruginosa* PA14 as previously described.[8] Briefly, cells were washed in 300 mM sucrose and electroporation of 500 ng plasmid DNA carried out at 2.5 kV, 25 µF, 200 Ω, using the Gene Pulser Electroporater (Bio-Rad). Transformants were selected on KB agar plates containing 30 ug gentamicin. The *egfp* expression in *Pseudomonas* was confirmed via measurements at 478/510 nm.

Plasmids used in this study: pBBR1.egfp.TIR: Cm^r, contains the TIR-*egfp*-T_0 cassette in pBBR1MCS in opposite orientation with respect to the *lac* promoter[6]; pMCh-23: Gm^r, Ap^r, carrying the *mCherry* red fluorescent gene[7]; pUCP23.egfp: Gm^r, Ap^r, carrying the *egfp* enhanced green fluorescent gene (present study).

***Biofilm assays*:** Biofilm flow cell studies were performed following previously established experimental protocols from the literature.[9, 10] All experiments were conducted under sterile conditions.

Overnight cultures of the GFP-labelled PA14 strain were grown in lysogeny broth (LB) in the presence of gentamicin (50 µg·mL^{-1}) and were diluted to an OD_{600} of approx. 0.05 prior to biofilm experiments. Biofilm assays were performed in BM2 (7 mM $(NH_4)_2SO_4$, 40 mM K_2HPO_4, 22 mM KH_2PO_4 (pH 7), 0.5 mM MgSO4, and 0.4 wt% glucose) in the presence of gentamicin (50 µg·mL^{-1}). Coated and uncoated substrates were placed adjacently within the same flow cell chambers (CFCAS0004, IBI Scientific) and connected to silicon tubing (VWR, 89068-468; 0.062 × 0.125 inch (inner and outer diameter), 0.032 inch wall thickness). The flow cell system was sterilized by pumping a 0.5% hypochlorite solution through the system using a Watson Marlow 205S multichannel peristaltic pump (at 0.5 rpm, 30 min). Afterwards, the experimental setup was rinsed with sterile water (at 0.5 rpm, 1 h) and BM2 medium (1 h). The flow cell chambers were inoculated with aliquots (400 µL) of the diluted overnight culture and left without flow for 3 h. Biofilm experiments were performed under continuous flow (2.4 mL·h^{-1}; approx. 0.5 rpm) for 72 h at 37 °C. Biofilm eradication assays were conducted on preformed biofilms (48 h), which were subsequently exposed to ciprofloxacin (320 ng·ml^{-1}) for additional 24 h. Additional staining with propidium iodide (5 µM; Live/Dead BacLight bacterial viability

kit, Thermo Fisher Scientific) was conducted prior to microscopy for visualization of surface-adherent dead cells.

Static biofilm studies were performed in BM2 (recipe above) supplemented with $FeSO_4$ (10 µM) and gentamicin (50 µg·mL^{-1}). BM2 was inoculated with aliquots of the overnight culture diluted to an OD_{600} of approx. 0.05. The polymer patterned Ti surfaces were placed in separate wells of a 24-well plate and were covered by the inoculated medium (1 mL). Biofilms were grown for 72 h at 37 °C, and the media was replaced after 24 and 48 h, respectively. The substrates were gently washed in phosphate buffered saline (PBS) (1×) prior to confocal imaging in order to remove planktonic bacteria.

Supplementary Figures

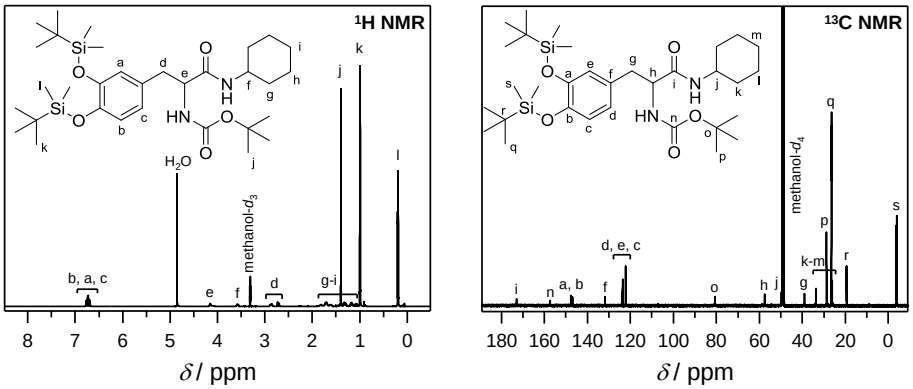

Fig. S1. ^{1}H NMR (600 MHz) and ^{13}C NMR (151 MHz) spectra (methanol-d_4, 298 K) of compound **3**.

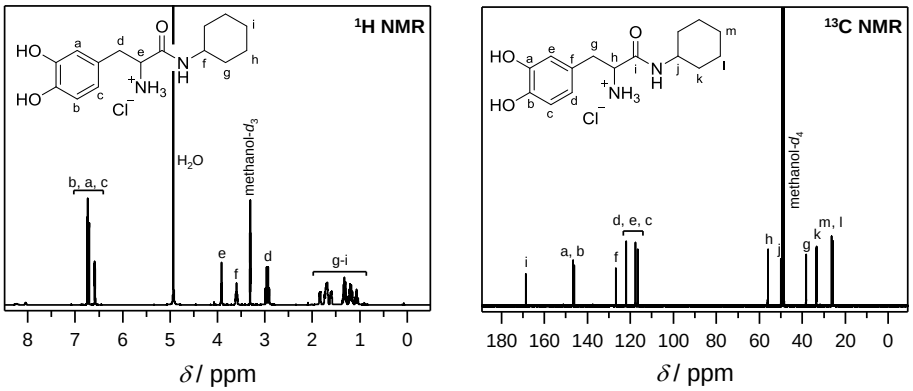

Fig. S2. ^{1}H NMR (600 MHz) and ^{13}C NMR (151 MHz) spectra (methanol-d_4, 298 K) of compound **5**.

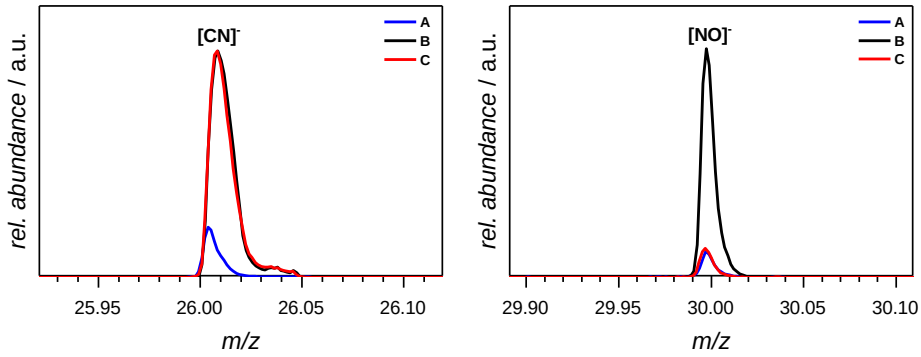

Fig. S3. (−)ToF-SIMS characterization of uncoated und polymer-coated HA surfaces **A–C**. The peak at *m/z* 26.01 was assigned to polymer-characteristic $[CN]^-$ fragments (*m/z*(theo) 26.00), detected on polymer-coated surfaces **B** and **C** (black and red solid lines). The nitroxide-characteristic $[NO]^-$ fragment at *m/z* 30.00 was detected easily on the TEMPO-functionalized surface **B**. Uncoated HA (surface **A**, blue solid line) and cyclohexyl-conjugated surface **C** did not show the nitroxyl-characteristic peak.

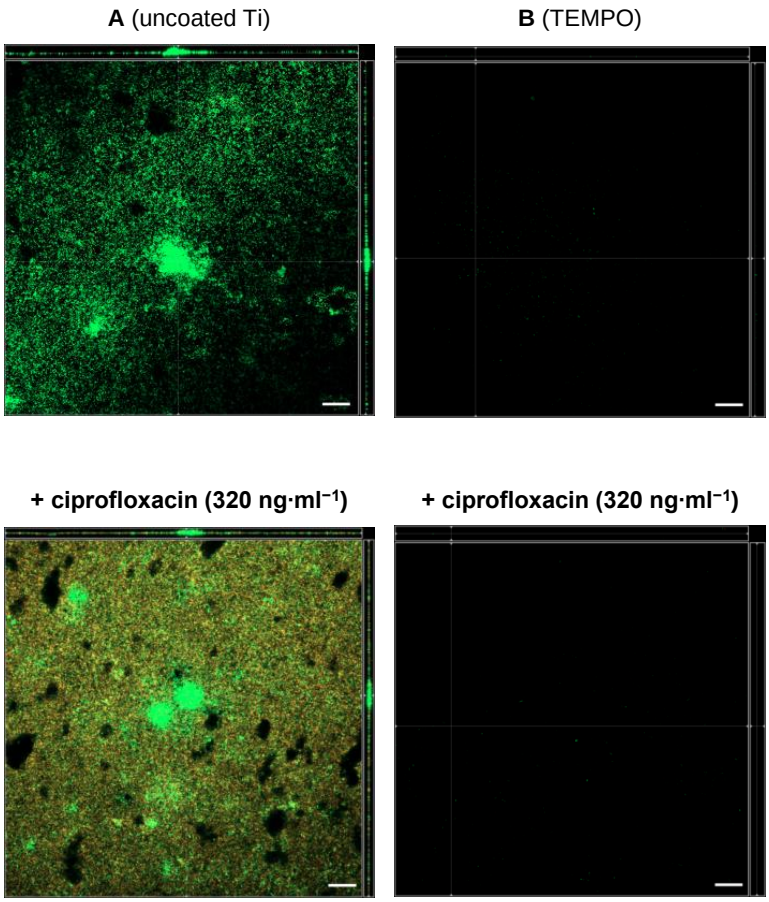

Fig. S4. *P. aeruginosa* biofilm cultivation on titanium with subsequent biofilm eradication experiments using antibiotic ciprofloxacin. Uncoated (**A**) and nitroxide polymer coated (**B**) titanium surfaces were exposed to PA14 surface colonisation for 72 h (top row) with addition of ciprofloxacin (320 ng·ml^{-1}) after 48 h of biofilm growth (bottom row). Biofilm assays were performed in a flow cell system at 37 °C. Dead bacteria were stained with propidium iodide (red) prior to confocal microscopy. Merged images composed of PI and GFP channels are displayed, and superimposed fluorescence response of live (green) and dead cells (red) appears yellow. The scale bars represent 50 µm in length. Each panel shows the *xy*, *yz* and *xz* dimensions.

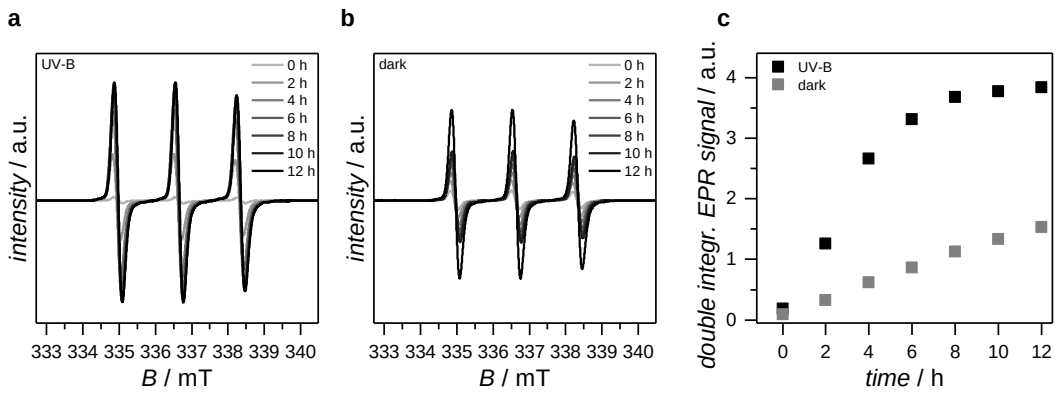

Fig. S5. EPR spectroscopic characterization of light-dependent nitroxide free radical formation during oxidative polymerization of **4** in Tris–HCl buffer (pH 8.5). a)–b) First-derivative EPR spectra of UV-B triggered aerobic hydroxylamine oxidation of **4**, complemented by control experiments performed in the dark. c) Time-resolved quantification of nitroxide-derived unpaired electron spins *via* double integration of the recorded EPR signals. The EPR spectra were simultaneously recorded during UV–vis spectroscopic analysis (refer to Fig. 4b).

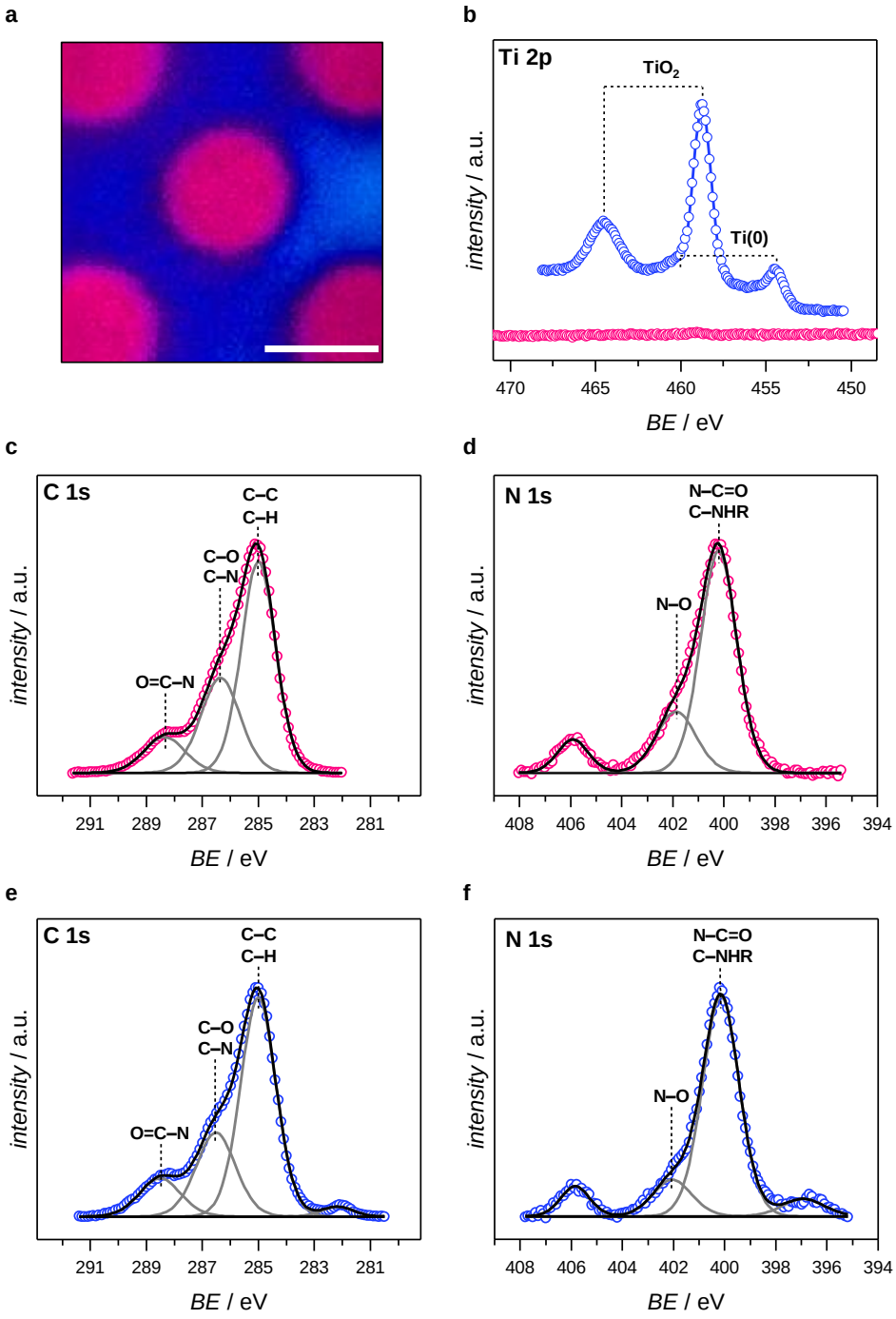

Fig. S6. In-depth XPS characterization of nitroxide polymer-patterned surface **D**. a) XPS overlay image constructed from substrate-derived Ti 2p XPS signals (blue) and polymer-derived C 1s XPS signals (magenta). Scale bar represents 1 mm in length. b) Ti 2p XP spectra obtained from polymer-conjugated (magenta) and nonconjugated areas (blue). c)–d) Corresponding C 1s and N 1s XP spectra of polymer-conjugated areas. The C 1s XP spectrum appeared to be identical compared to previously shown XP spectra (refer to Fig. 2). Likewise, the deconvolution of the N 1s XP spectrum showed a similar chemical composition in correspondence to previous results. However, the additional peak at higher BEs (405.9 eV) was particularly pronounced indicating the presence of higher oxidized N-containing species, e.g. *N*-oxoammonium cations.[5] The prolonged UV exposure during the photopolymerization of **4**, most likely, triggered the overoxidation of the nitroxide functional group (initially present as the

hydroxylamine hydrochloride salt). e)–f) Corresponding C 1s and N 1s XP spectra of areas which have been covered by the shadow mask. Both spectra confirmed the omnipresence of thin polymer films deposited on the surface, however less abundant in areas which have been shielded from UV irradiation (refer to b)). This observation indicates that the polymer surface deposition cannot be suppressed with this photolithographic coating setup due to polymer diffusion and unspecific polymer–substrate interactions.

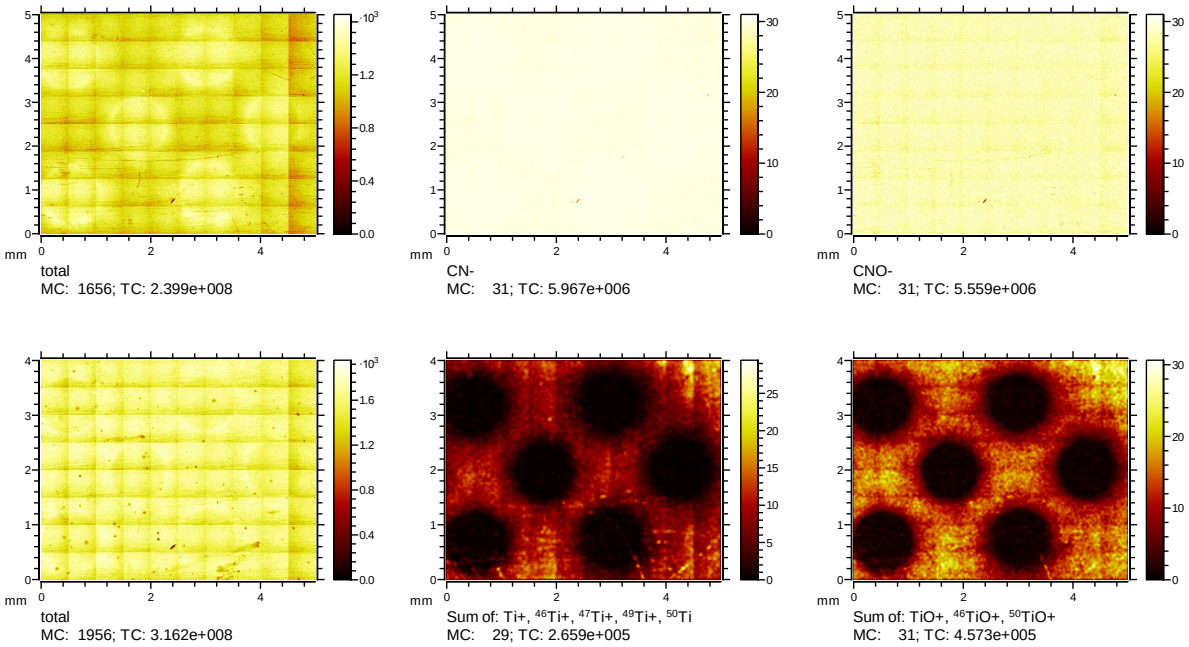

Fig. S7. Static ToF-SIMS characterization of polymer-patterned surface **D**. Imaging of polymer-characteristic $[CN]^-$ and $[CNO]^-$ fragments[11] (top row) and several Ti isotopes derived from the underlying substrate (bottom row). As clearly shown, a direct imaging of the polymer pattern by static SIMS is hampered by the very low probing depth (in the range of 2–5 nm) and by the onset of signal saturation for the strong $[CN]^-$ and $[CNO]^-$ signals. Therefore, the image contrast of the polymer peaks is quite low. Weak substrate peaks are detectable (please note that the count rates (TC total counts of the given secondary ions in the field of view) are about one order of magnitude lower as compared to $[CN]^-$ and $[CNO]^-$), leading to the conclusion that a very thin adsorbate layer has also formed in between the irradiated spots. Ti and TiO images were 4 pixel binned to increase the dynamic range on the expense of reduced lateral resolution.

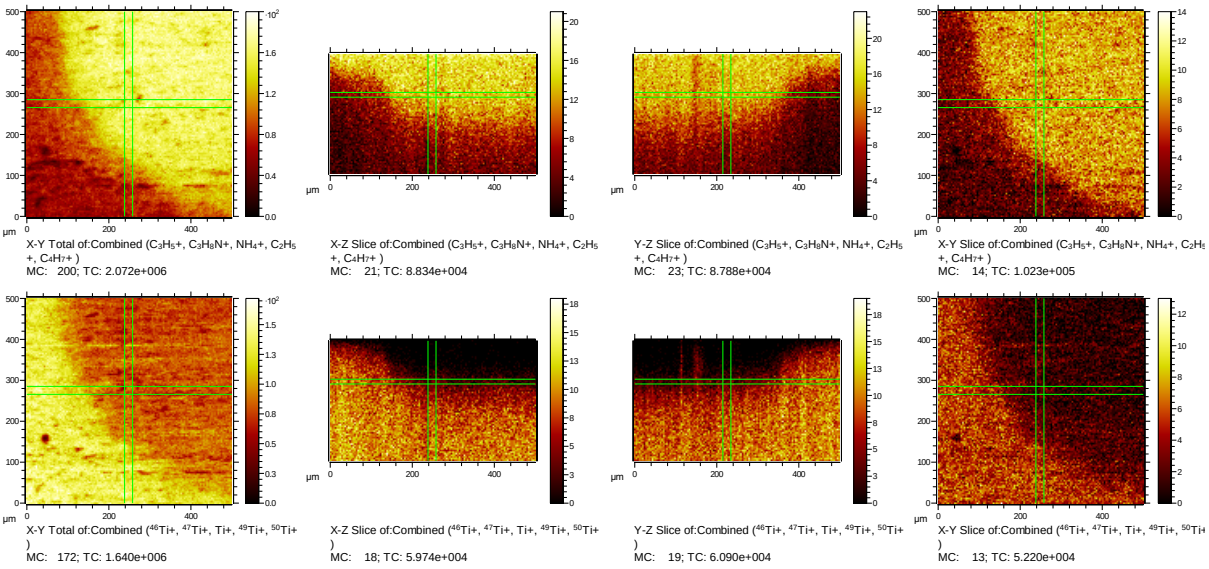

Fig. S8. Dynamic ToF-SIMS characterization of polymer-patterned surface **D**. Both leftmost images show the lateral distribution of the depth-integrated signals of some fragments characteristic for the polymer layer, hydrocarbons and NH_4^+ (top row), and for the underlying Ti substrate (bottom row), respectively. The *xz* and *yz* cross sections are depicted in the central images, and the *xy* slices along the green lines are depicted in the rightmost images.

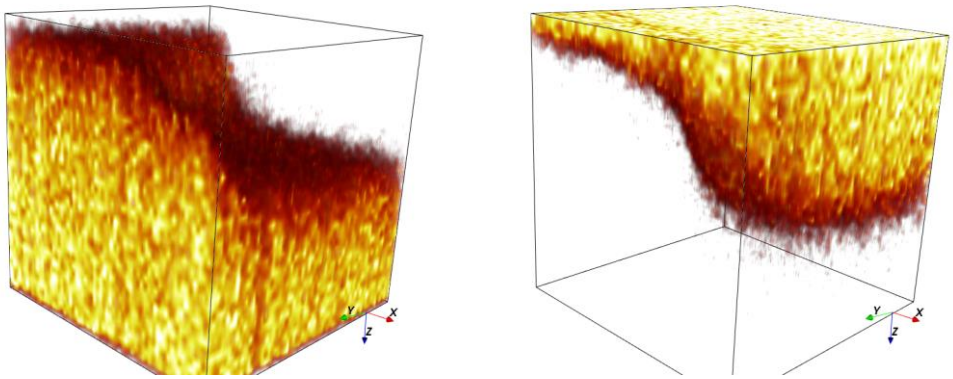

Fig. S9. ToF-SIMS 3D rendering of Ti signals (left image, sum of all isotopes) and polymer fragments (right image, sum of $[C_2H_5]^+$, $[C_3H_5]^+$, $[C_4H_7]^+$, $[C_2H_5N]^+$, and $[NH_4]^+$ fragments). The intensities are indicated by a heat scale. The *x* and *y* range are 500 µm (black box), the *z* range is not to scale.

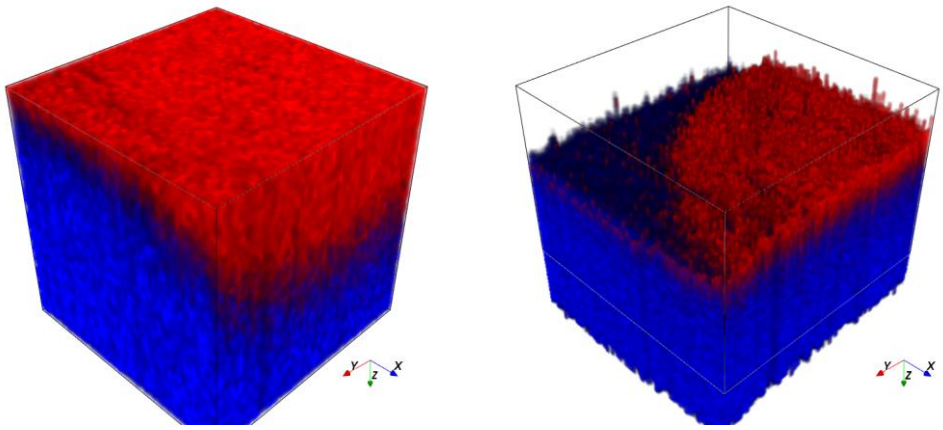

Fig. S10. ToF-SIMS color-coded 3D rendering and overlay of Ti signals (blue) and polymer signals (red). The data representation (left image) is based directly on obtained raw data, hence showing a flat topmost surface of the sample, which does not hold true for this specimen. Rather, the underlying titanium substrate can be regarded as being flat on the 500 × 500 µm^2 area (with only random surface roughness features). Therefore, the dataset can be rearranged in a way that for voxels representing the Ti signals reaching a predefined threshold intensity the level is set to an equal *z* value, and all other voxels are referenced to that *z* level. In practice, a certain voxel binning was required to increase the dynamic range and to reduce noise. A *xy* binning of 4 pixel and a *z* binning of 2 was applied and setting the threshold intensity for Ti as high as possible but still reached by all (binned) voxel. The height compensation to level out the Ti surface is shown at the bottom of the right image. The *x* and *y* range are 500 µm (black box), the *z* range is not to scale.

References

1. C. Lang, S. Bestgen, A. Welle, R. Müller, P. W. Roesky and C. Barner-Kowollik, *Chem. Eur. J.*, 2015, **21**, 14728-14731.
2. K. L. Parry, A. G. Shard, R. D. Short, R. G. White, J. D. Whittle and A. Wright, *Surf. Interface Anal.*, 2006, **38**, 1497-1504.
3. J. H. Scofield, *J. Electron. Spectrosc. Relat. Phenom.*, 1976, **8**, 129-137.
4. B. P. Lee, K. Huang, F. N. Nunalee, K. R. Shull and P. B. Messersmith, *J. Biomater. Sci., Polym. Ed.*, 2004, **15**, 449-464.
5. H. Woehlk, J. Steinkoenig, C. Lang, L. Michalek, V. Trouillet, P. Krolla, A. S. Goldmann, L. Barner, J. P. Blinco, C. Barner-Kowollik and K. E. Fairfull-Smith, *Langmuir*, 2018, **34**, 3264-3274.
6. A. Burse, H. Weingart and M. S. Ullrich, *Mol. Plant-Microbe Interact.*, 2004, **17**, 43-54.
7. C. L. Berry, A. K. C. Brassinga, L. J. Donald, W. D. Fernando, P. C. Loewen and T. R. de Kievit, *Can. J. Microbiol.*, 2012, **58**, 1027-1034.
8. D. Pletzer, Y. Braun and H. Weingart, *Antonie van Leeuwenhoek*, 2016, **109**, 737-753.
9. C. de la Fuente-Núñez, F. Reffuveille, K. E. Fairfull-Smith and R. E. W. Hancock, *Antimicrob. Agents Chemother.*, 2013, **57**, 4877-4881.
10. F. Reffuveille, C. de la Fuente-Núñez, K. E. Fairfull-Smith and R. E. W. Hancock, *Pathog. Dis.*, 2015, **73**, ftv016.
11. X. Du, L. Li, J. Li, C. Yang, N. Frenkel, A. Welle, S. Heissler, A. Nefedov, M. Grunze and P. A. Levkin, *Adv. Mater.*, 2014, **26**, 8029-8033.